Characterising tissue outcomes and the neuroinflammatory response following a thoracic porcine spinal cord injury

A thesis submitted in partial fulfilment of the

HONOURS DEGREE of BACHELOR OF

HEALTH AND MEDICAL SCIENCES In

The Discipline of Pathology

Adelaide Medical School

By Ryan Dorrian

November 2020

Abstract

Background: Clinical translation of promising therapeutic interventions for spinal cord injury (SCI) remains poor, potentially due to discrepancies between rodent and human SCI pathophysiology. A porcine model could serve as an intermediary model, given greater similarity to human pathophysiology, thus potentially improving translation.

Gaps in knowledge: We have developed the first domestic porcine model of SCI within Australia. However, tissue outcomes for graded SCI severities have not been characterised. This is required to better understand the relationship between severity and outcomes and ultimately guide the development of therapeutic interventions. Additionally, the microglial response to SCI needs to be characterised to facilitate therapeutic research aiming to modulate neuroinflammation.

Methods: A porcine T10 contusion/compression SCI was induced via a weight drop injury device. Drop height varied between 20cm (n=4) and 10cm (n=3) to induce graded SCI severities. Spinal cords were extracted 14 days post-SCI, and processed for histological analysis using haematoxylin and eosin and luxol fast blue (morphology and lesion volume) and IBA-1 (microglial expression) immunohistochemistry.

Results: Lesion volume was significantly greater in the 20cm than 10cm SCI ($p=0.029$), suggesting a greater injury severity was induced. Microglial expression was elevated compared to sham, particularly at the injury epicentre ($p<0.0001$), but there were no significant differences between severity groups.

Conclusion: We were successful in characterising the first porcine SCI model in Australia, and characterised the extent of tissue damage at graded SCI severities. While microglial activity did not differ between severity groups, we have provided significant groundwork for future characterisation of the model.

Word Count = 250

Introduction

Annually, 200-400 Australians are devastated by the debilitating motor, sensory and autonomic functional loss caused by a traumatic spinal cord injury (SCI)[1]. The drastic consequences of SCI significantly impinge on quality of life[2], often leaving the individual with permanent disability due to the lack of effective treatments[3]. Despite a significant number of human clinical trials, no treatment to date has shown meaningful increases in functional outcomes or neurological recovery following injury[4, 5]. This limited success may be due to discrepancies between rodents and human SCI pathophysiology[6, 7]. Hence, there is a critical need to develop alternative models for SCI research that more accurately replicate human SCI conditions[7].

SCI Pathophysiology

SCI pathophysiology is biphasic, consisting of the primary injury and a subsequent vascular, cellular and inflammatory secondary injury cascade[8]. The most common characteristic of the primary injury is an initial impact (contusion) followed by bony compression of the spinal cord[9], resulting in significant tissue damage through haemorrhaging and necrotic cell death[10]. Unfortunately, this primary injury occurs instantaneously and is not amenable to intervention. However, the initial injury sets in motion the secondary injury cascade that occurs over a delayed timeframe and may be treatable[5].

A significant component of secondary injury is the neuroinflammatory response. As resident immune cells of the spinal cord, microglia are among the first responders and become activated within minutes following SCI. This activation causes a morphological change within the microglia (Figure 1)[11], which become phagocytic and rapidly migrate to the lesion site[12]. There, microglia clear cellular debris through phagocytosis, and contribute to the formation of a glial scar that surrounds the injury site[13]. Microglia can also release anti-inflammatory cytokines (IL-4, IL-12) that are beneficial, promoting neurogenesis and tissue repair[14]. Taken together, these functions are vital for regaining homeostasis and are considered necessary for recovery.

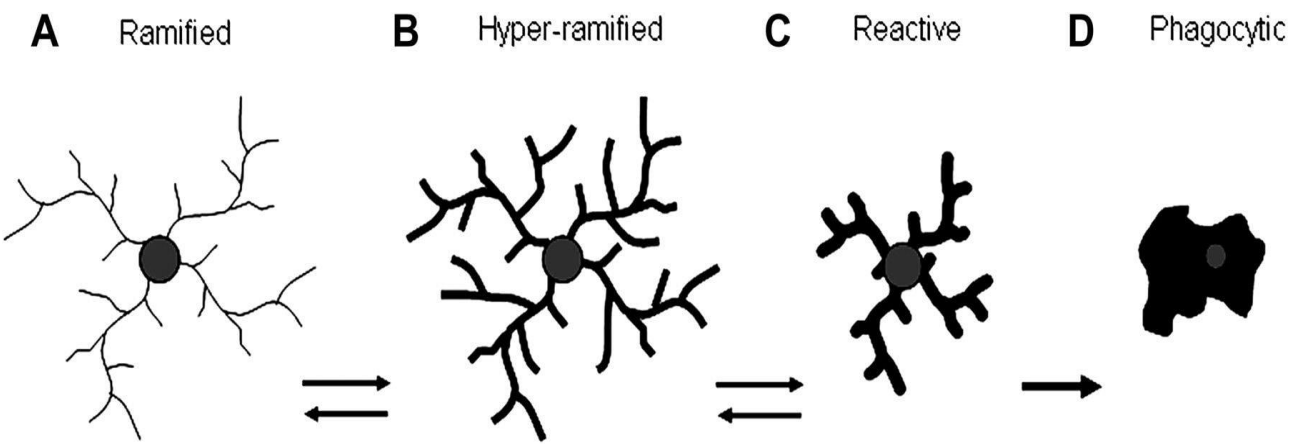

Figure 1: Microglia initially exhibit a ramified morphology with many fine projections (A), which become thicker and shorter as microglia become more reactive (B, C). Phagocytic microglia have an amoeboid appearance with few processes remaining (D).[15]

Despite these beneficial functions, activated microglia also release detrimental factors that can damage spared tissue adjacent to the injury site and expand the lesion[16]. For example, microglia release nitric oxide and reactive oxygen species that can interact with neighbouring cells, causing mitochondrial dysfunction, DNA damage, and cell death[17, 18]. Additionally, microglia can release pro-inflammatory cytokines (TNF-α, IL-1β, IL-6) that promote the influx of additional immune cells to the injury site[19], enhancing production of oxidative metabolites and causing further non-specific damage[20]. Thus, there is clear therapeutic potential in limiting these detrimental functions and modulating neuroinflammation towards a neurotrophic response[21].

SCI Animal models

While our understanding of SCI pathophysiology has vastly improved, the majority of this information has stemmed from rodents[22]. Unfortunately, treatments proven efficacious in rodent research have generally failed in human clinical trials – highlighting the possibility that rodent and human pathophysiology may differ[4]. Indeed, inflammatory cytokine expression persists for a shorter duration and peaks earlier in rodents, suggesting the rodent neuroinflammatory response may vary to humans[23-25]. Additionally, substantial differences in spinal cord length and calibre further limit translatability[26].

As such, porcine SCI models have been suggested, and exhibit numerous advantages that make it a potential intermediary model to bridge rodent and human trials[26, 27]. Pigs are extensively used in immunological research due to their similar immune structure to humans[28], which suggests the neuroinflammatory response to SCI may also be similar[29]. Indeed, porcine microglial activation and function closely resemble humans, with comparable amounts of oxygen free radicals, nitric oxide, IL-1β, and TNF-α released after noxious immune stimulation via lippopolysaccharides[30]. Circulating white blood cell counts are similar between pigs and humans, particularly for neutrophils[31], which are known to play a significant role post-SCI[32]. The spinal anatomy of pigs closely resembles humans – especially at the T6 to T10 regions[33] – with spinal cord size and the organisation of white matter tracts within the cord closely akin to humans[29, 34, 35]. Thus, the porcine SCI model an attractive option, particularly for neuroinflammatory research.

Gaps in knowledge

While there are clear advantages, the porcine model remains underutilised. This was highlighted in a 2017 review of animal SCI research, which found that only 1.5% of studies were conducted in porcine models[36]. Indeed, the usability of existing porcine SCI models is limited by the global availability of the breeds of pigs[37]. Despite well-characterised models existing for both Yucutan[27] and Gottingen-Minnesota minipigs[38], these breeds are unavailable within Australia. Consequently, there is currently no porcine SCI models available within Australia, limiting the ability for researchers to conduct necessary translational research. We have developed a domestic porcine SCI model; however, the model requires extensive characterisation. Notably, we are yet to characterise the extent of tissue damage following graded SCI severities. It is vital that we understand the impact of SCI severity on tissue outcomes, as there is immense variability in human SCI severity that must be considered when developing potential treatments[39]. Thus, this knowledge gap must be addressed before our porcine model is applied for therapeutic research. Additionally, the neuroinflammatory response both in our model and existing porcine SCI models has received little attention, with changes in the expression of microglia at various severities not characterised. Since there is clear therapeutic potential in

modulating neuroinflammation towards a neuroprotective state, this response must be well characterised within this potential pre-clinical model[40].

Hypothesis and Aims

To address these knowledge gaps, we investigated lesion volume and the neuroinflammatory response at different SCI severities within our porcine T10 SCI model. We hypothesised that there would be a greater neuroinflammatory response and subsequently greater tissue damage following a 20cm than a 10cm contusion/compression SCI. The following aims were developed to analyse this hypothesis:

Aim 1: Characterise the extent of tissue sparing and lesion volume within the spinal cord after a 20cm and 10cm contusion/compression SCI.

Aim 2: Characterise the impact of SCI severity on the microglia response within the spinal cord at 14 days post-SCI.

Methods

Animal procedures were approved by The University of Adelaide and South Australian Health and Medical Research Institute ethics committees (SAM 243, 24/1/17), and were conducted according to the NHMRC Australian Code for the Care and Use of Animals for Scientific Purposes (8th edition, 2013).

Female domestic pigs (n=7) weighing 20-30kg arrived 14 days before SCI induction. Animals were individually housed and fed twice daily with access to water *ad libitum*, and were randomly allocated into SCI severity groups (Table 1). Sham animals underwent all procedures but did not receive an SCI. This tissue was archival and taken at 24 hours post-SCI induction surgery, and was used for comparisons between severity groups for IBA-1 immunoreactivity.

Drop Height	Sample Size
Sham	n=3
10cm	n=3
20cm	n=4

Table 1: Overview of SCI severity groups

Surgical Procedures

The study timeline (Figure 2) commenced with animal arrival 14 days pre-SCI. Central lines were placed five days before SCI induction (day 0). Animals were then closely monitored for 14 days, before being humanely killed via intracardial perfusion.

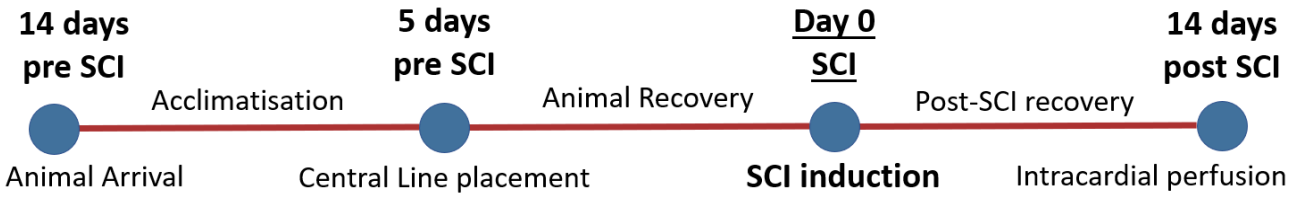

Figure 2: Timeline of study design, highlighting the major events.

Animals received medetomidine (0.02-0.04mg/kg), ketamine (11mg/kg) and propofol (2mg/kg) to induce general anaesthesia. Anaesthesia was maintained via a constant intravenous ketamine (7.0-8.0mg/kg/hr), propofol (3.5-4.5mg/kg/hr), midazolam (0.1-0.2mg/kg/hr) and fentanyl (6.0-8.0µg/kg/hr) infusion. Following induction, the pigs were endotracheally intubated, and heart rate, blood pressure, oxygen saturation and rectal temperature monitored throughout all procedures.

Central Line Placement

Catheters were inserted into the external jugular vein for intravenous medication delivery and venous blood sampling, and into the internal carotid artery for blood pressure monitoring and blood gas analysis (Figure 3).

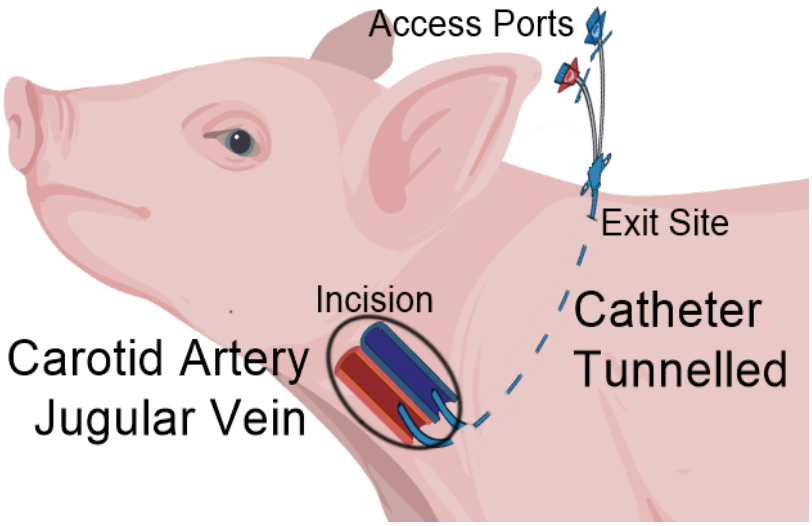

Figure 3: Schematic overview of central line placement surgery. Image adapted from Lombardo et al. 2010[41]. Created at BioRender.com

A 2cm incision was made on the left neck (Figure 4A), and two catheters were subcutaneously tunnelled from this incision and externalised on the dorsal midline of the pig. Blunt dissection was used to locate the external jugular vein, which was occluded with silk tie (2-0), incised, and a catheter inserted 10cm into the vessel. The silk tie was then used to secure the catheter in the vessel (Figure 4B). This was repeated to catheterise the internal carotid artery, before suturing the wound closed by anatomical layer.

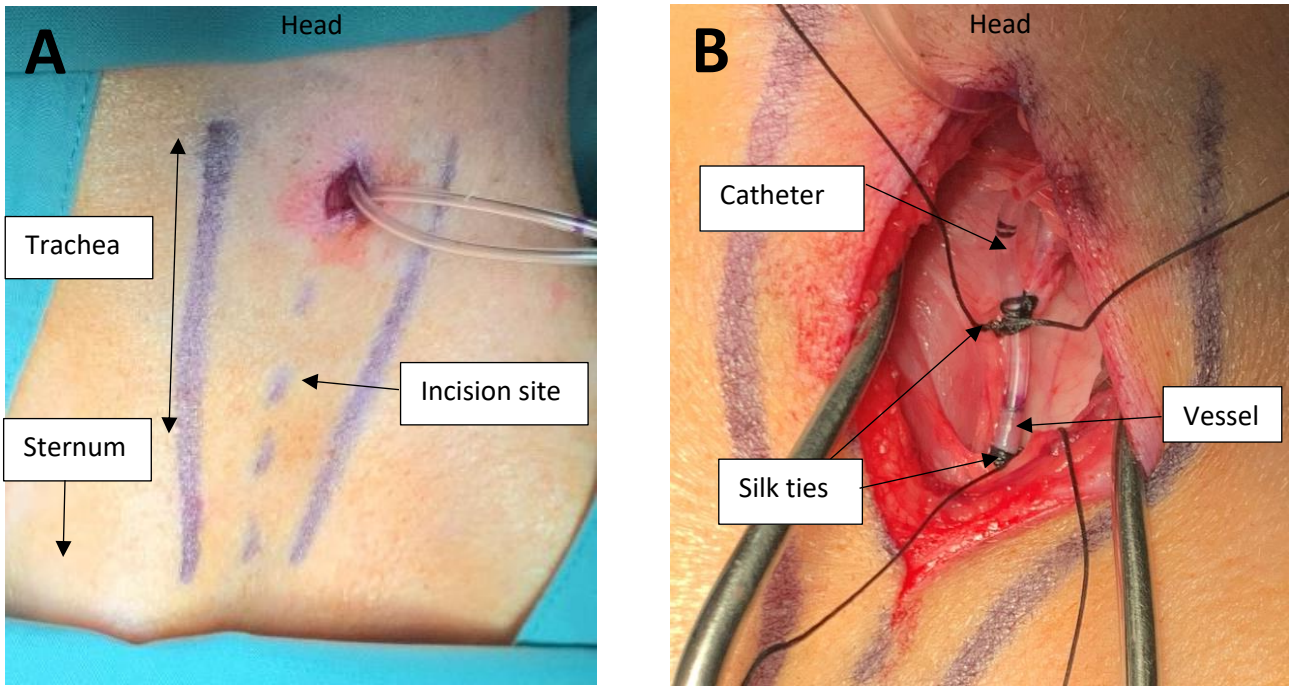

Figure 4. Central line placement surgery: **(A)** Guidance lines along jugular groove for incision to locate jugular vein and carotid artery. **(B)** Catheter inserted into vessel and secured using silk tie.

CT Scan

Animals underwent a supine axial CT scan (Philips Brilliance 16 Slice CT scanner) to count the number of thoracic vertebrae, which varies between 15 and 16 for domestic pigs[42].

Spinal Cord Injury Induction (Figure 5)

Animals were placed in a prone position on the operating table, and T10 located via a C-arm fluoroscopy scan by counting thoracic vertebrae. A dorsal midline incision was made from T9 to T14, and the muscle retracted. The spinous processes from T9-T13 were removed, and a T10 laminectomy performed to expose the spinal cord (Figure 6A). Pedicle screws were placed bilaterally at T12 and T13 to mount a custom weight-drop injury device (Figure 6B). A contusion SCI was induced by dropping a 50g impactor weight onto the exposed T10 spinal cord from 10cm or 20cm, as previously recommended to induce a mild or moderate SCI respectively[43]. An additional 100g weight was added for 5 minutes to mimic bony compression seen clinically[9]. The injury device and pedicle screws were then removed, and the wound sutured closed by anatomical layer.

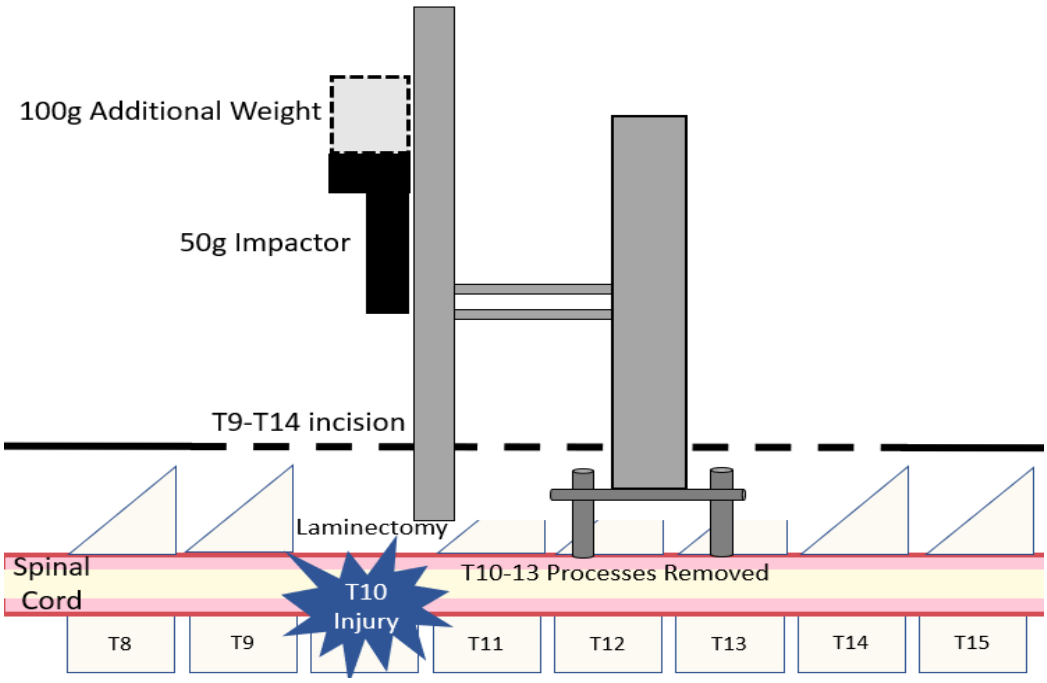

Figure 5: Schematic overview of SCI induction surgery.

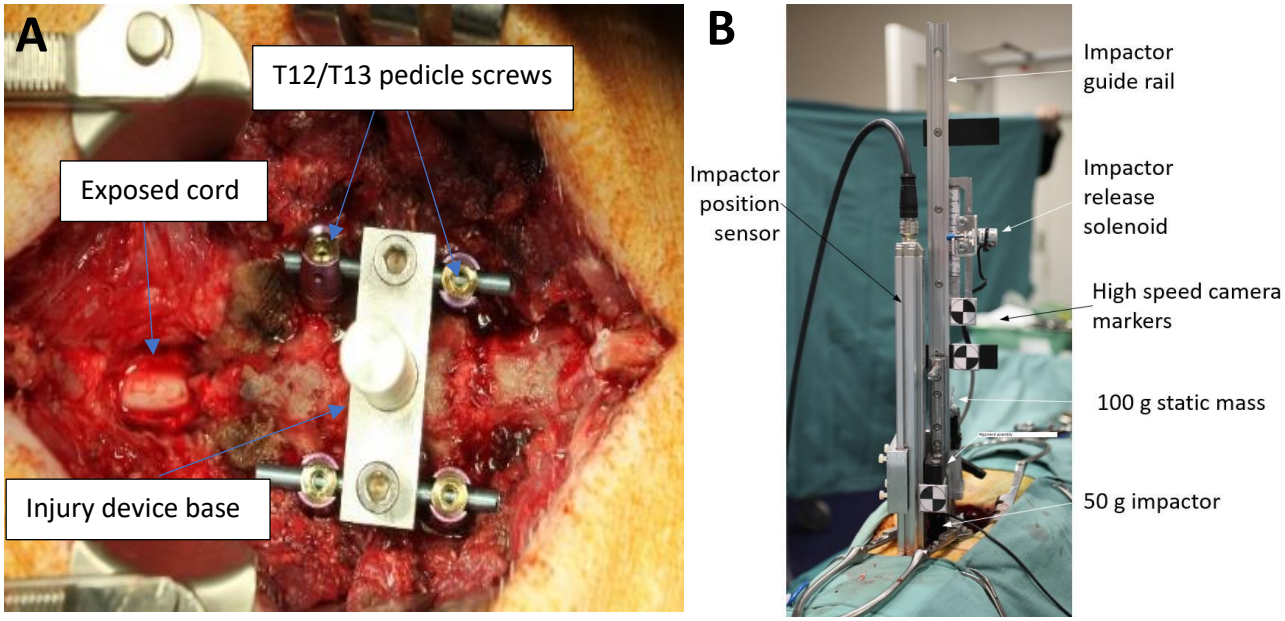

Figure 6: Injury device for SCI induction. **A:** Exposed spinal cord after T10 laminectomy and pedicle screw placement **B:** Custom weight drop injury device for SCI induction.

Histological Methods

14 days post-SCI, animals were humanely killed via a 1L intracardial saline perfusion and subsequently fixed with a 2.5L 10% buffered formalin perfusion. The spinal cord was extracted and post-fixed in 10% buffered formalin for two weeks. Afterwards, spinal cords were cut into 1cm sections centred about the injury epicentre, before being processed and embedded in paraffin wax.

Paraffin blocks containing the injury site were serially sectioned; 5µm thickness and 500µm apart, allowing for lesion volume calculations. Additional sections were cut at 3cm, 5cm and 10cm both cranially and caudally to the injury epicentre (Figure 7).

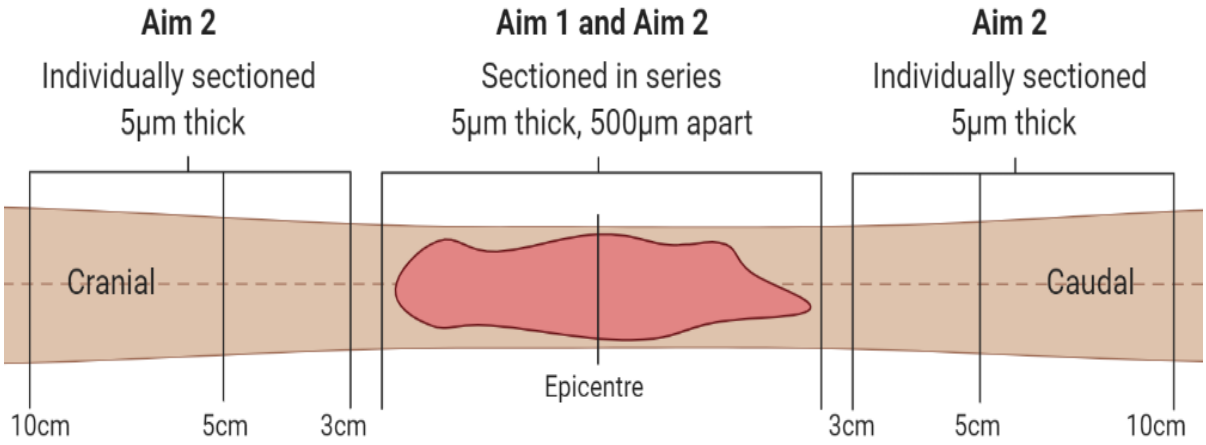

Figure 7: Spinal cord histological sectioning.

Lesion volume Analysis

Lesioned spinal cord segments were stained with haematoxylin, eosin and luxol fast blue (H&E-LFB) to observe grey and white matter morphology respectively. We defined grey matter lesion as absent tissue, or tissue with haemorrhaging present (Figure 8A), and white matter lesion as absent tissue, or as regions of severe myelin vacuolation (Figure 8B). Slides were scanned using a Hamamatsu Nanozoomer (v2.0R) and damaged tissue manually segmented using the Nanozoomer Digital Pathology program (Hamamatsu, v2.7.39) to determine lesion area. The percentage of tissue sparing and lesion volume were then calculated using the following formulas:

$$Percentage\ Tissue\ Sparing = \frac{total\ spinal\ cord\ area - lesion\ area}{total\ spinal\ cord\ area} \times 100\%$$

$$Lesion\ Volume\ (mm^3) = \sum lesion\ area\ (all\ segments)\ \times 0.5mm\ (distance\ between\ segments)$$

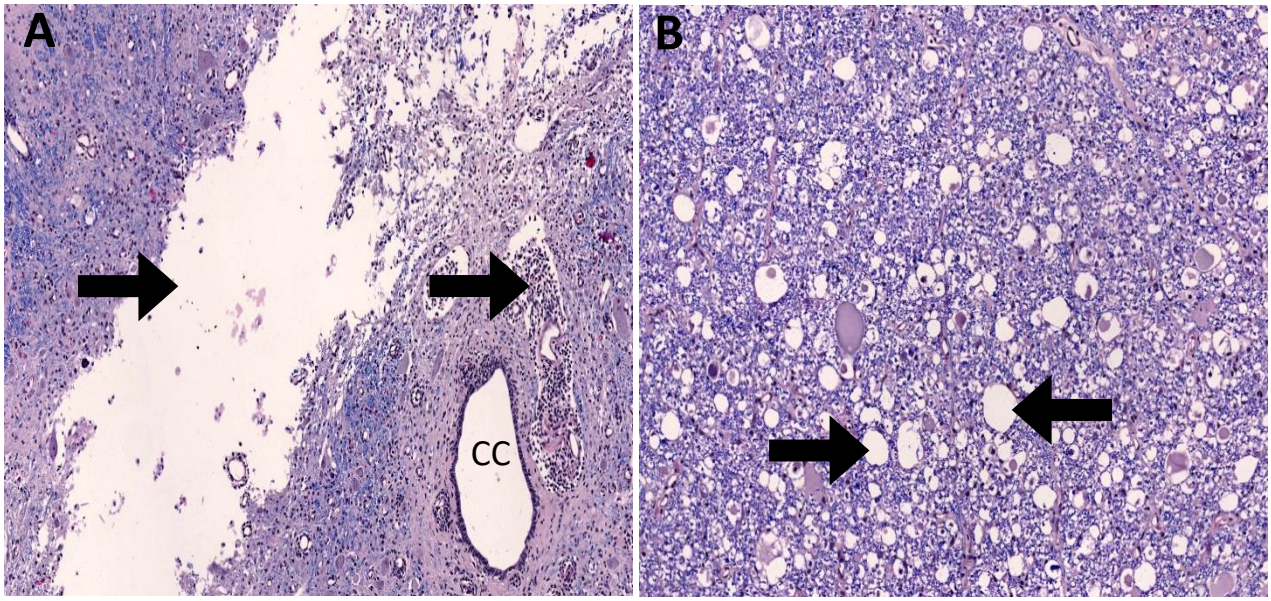

Figure 8: Morphological damage observed within injury site. **(A)** Arrows indicate absent or unnatural grey matter tissue. CC=Central Canal. **(B)** Arrows indicate myelin vacuolation in white matter post-SCI.

IBA-1 Immunohistochemistry

Injury epicentre spinal cord segments (0cm) and segments 10cm, 5cm, 3cm, 1cm cranially and caudally to the epicentre were routinely deparaffinised and endogenous peroxidases blocked (1.5% hydrogen peroxide in methanol, 30 minutes). Antigen binding sites were revealed by heat-induced epitope retrieval in a citrate buffer, and non-binding sites blocked with normal horse serum (Vector, S-2000-20). The primary antibody – goat IBA-1 polyclonal antibody (Invitrogen, PA5-18039, 1:1000) – was applied overnight before washing slides three times (0.1% Triton-X in PBS) and applying the secondary antibody horse anti-goat IgG (Vector, BA-9500-1.5) for 30 minutes. Slides were then washed and incubated with Streptavidin Peroxidase Conjugate (Vector, SA-5004-1, 1:1000) for one hour. 3,3'-diaminobenzidine (DAB) (Vector, SK-4100) was used for colouration, and haematoxylin used as a counterstain.

Slides were scanned and region of interests exported using a 20x lens (Figure 9). Images were imported into ImageJ (v1.53c, National Institute of Health) and processed with a colour deconvolution plugin to visualise DAB staining. An automated cell count was conducted by thresholding the images (0-120) and running a particle analysis (size 125-2000). Due to the intensity of staining and tissue disruption, epicentre regions were manually counted using QuPath (v0.2, University of Edinburgh[44]).

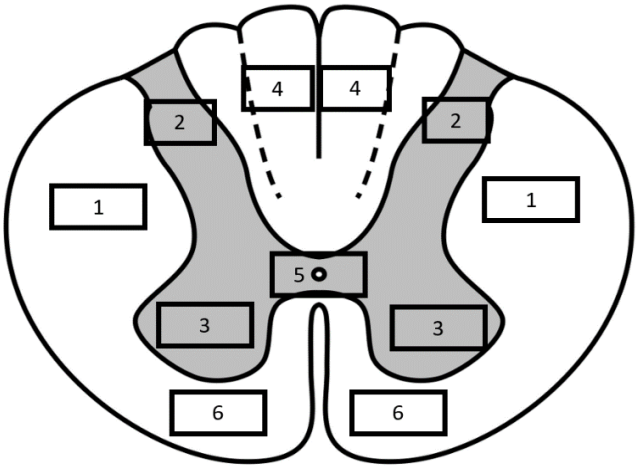

Figure 9: Regions of interest for IBA-1 analysis. 1: Lateral Columns, 2: Dorsal Horns, 3: Ventral Horns, 4: Dorsal Columns, 5: Central Canal, 6: Ventral Columns.

Statistical analysis

Statistical analysis was conducted using the GraphPad Prism software (v8.0.0). Non-parametric Mann-Whitney U tests were used to compare SCI severities for tissue sparing and total lesion volume, as data were not normally distributed. Due to the lack of a non-parametric test to compare two independent variables, a repeated measures two-way ANOVA with severity as a between-groups factor and region as a within-groups factor was used to compare lesion volume and IBA-1 immunoreactivity. To compare grey and white matter lesion percentage, a repeated measures two-way ANOVA with both region and grey/white matter as within-group factors was used. Sidak's multiple comparisons were used for all analysis. Significance was defined as $p<0.05$, and data are represented as mean ± SD.

Results

All surgical procedures were conducted with no major complications, and all animals were included in our analysis.

Tissue Sparing Analysis

H&E-LFB staining demonstrated marked damage (disruption of tissue architecture) to the injury epicentre and adjacent regions for both injury severities (Figure 10). Notably, damage within the 20cm group persisted at 9mm cranially and caudally, whereas the lesion appeared contained at 6mm for the 10cm SCI.

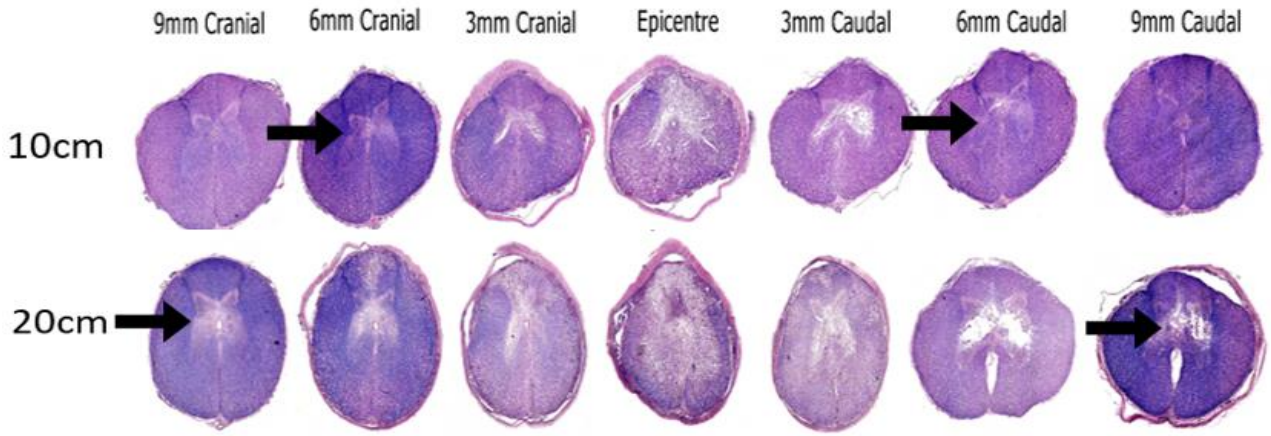

Figure 10: H&E-LFB staining demonstrating the extent of lesion. Arrows indicate the segment with the last visible lesion present for each severity.

Percentage Tissue Sparing

The percentage of tissue sparing (Figure 11) followed a similar pattern for both severities, exhibiting minimal tissue sparing at the epicentre (20cm: 0±0mm^3, 10cm: 3.67±6.35mm^3) which increased in distal segments. Significantly greater tissue sparing was observed for the 10cm SCI cranially (5mm, 9mm) and caudally (2-7mm) ($p<0.05$), indicative of reduced tissue damage. Notably, the lower area under the curve for the 20cm SCI suggests an overall reduction in tissue sparing.

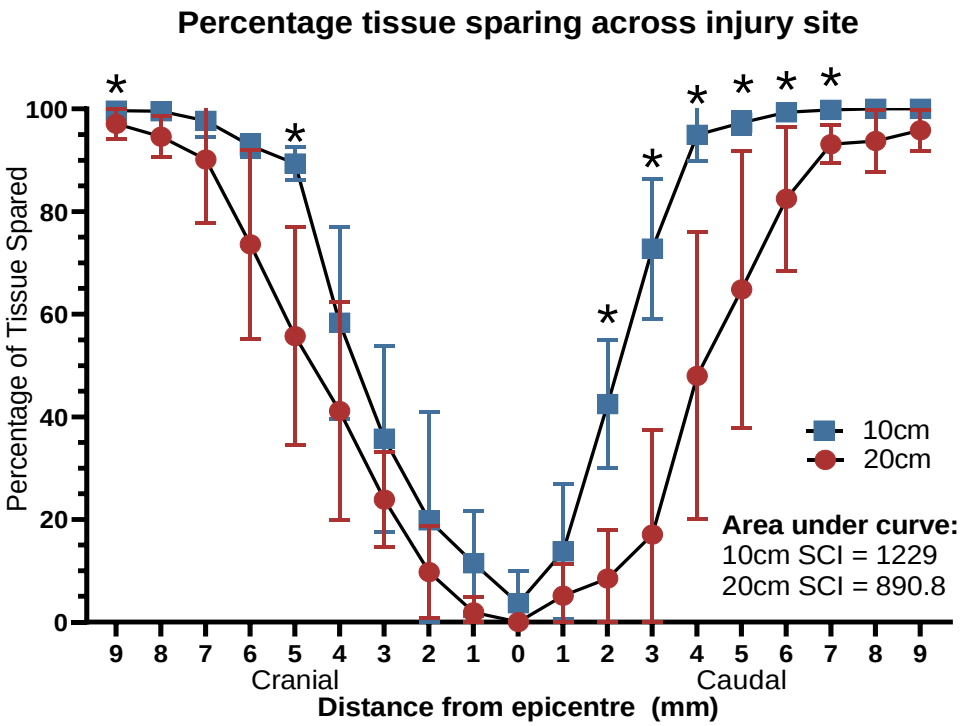

Figure 11: Tissue sparing analysis. Significant differences ($p<0.05$) between severities were observed at 9mm and 5mm cranially, and at 2-7mm caudally (denoted by *).

Lesion Volume Analysis

The 20cm SCI resulted in significantly greater total lesion volume (250.1 ± 56.66mm^3, p=0.03) than the 10cm SCI (133.9 ± 17.27mm^3), further indicating a greater extent of injury (Figure 12A). Despite a significant main effect for SCI severity (p=0.02), there were no significant differences between severities in the cranial (p=0.10), epicentre (p=0.30), or caudal (p=0.09) regions (Figure 12B). For the 10cm SCI, the epicentre was significantly elevated compared to adjacent regions (cranial: p=0.02, caudal: p=0.04), while the epicentre was significantly greater than the cranial region (p=0.02) for the 20cm SCI.

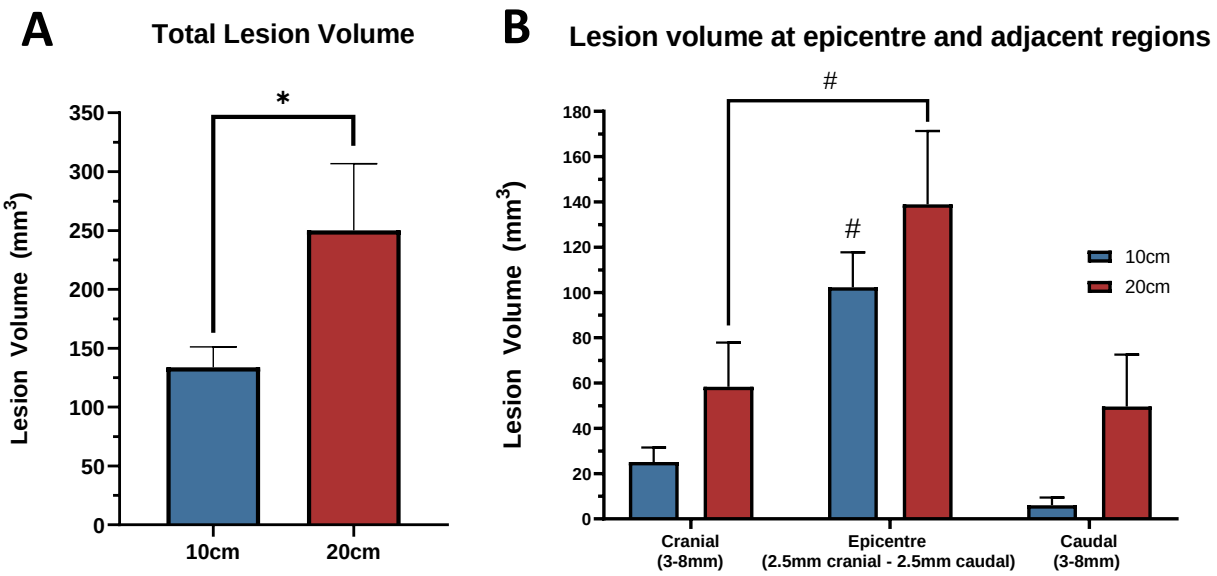

Figure 12: Lesion volume comparisons between severities. **(A)** A Mann-Whitney U test revealed a significantly greater total lesion volume for the 20cm SCI than the 10cm ($p=0.03$). **(B)** While a repeated-measures two-way ANOVA revealed a significant main effect between severities ($p=0.02$), pairwise comparisons revealed no significant differences between severities cranially ($p=0.10$), at the epicentre ($p=0.30$) or caudally ($p=0.09$). There was a significant main effect for region ($p=0.0003$), which was between the epicentre and cranial region for the 20cm SCI ($p=0.016$), and epicentre compared to cranial ($p=0.02$) and caudal ($p=0.04$) regions for the 10cm SCI (denoted by #).

Grey and White Matter Lesion Volume

There was a significant main effect for region in both the 10cm (Figure 13A) and 20cm groups (Figure 13B) ($p<0.0001$), with the percentage of lesion volume significantly greater in the epicentre than adjacent regions for both grey and white matter ($p<0.0001$). There were no significant differences between grey and white matter for the 10cm SCI (main effect $p=0.08$). However, there was a significant main effect between tissues for the 20cm SCI ($p=0.047$), with the percentage of grey matter lesion volume significantly higher than white matter caudally ($p=0.011$).

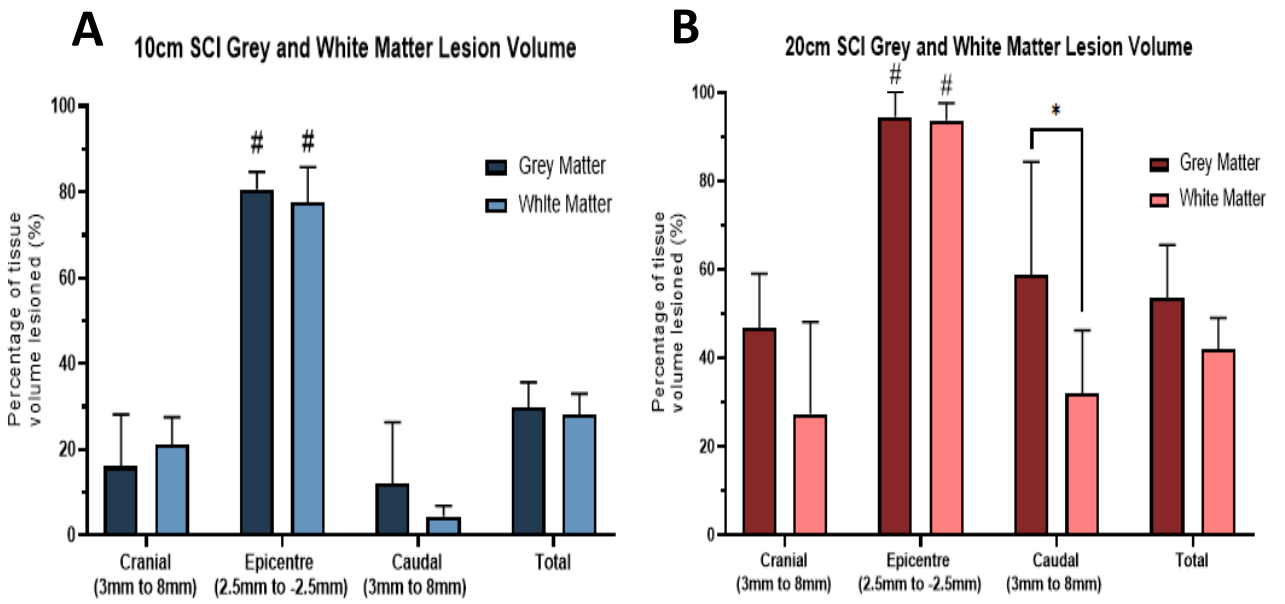

Figure 13: Grey and white matter percentage lesion volume. **(A)** For the 10cm SCI, a significant main effect for regions was observed ($p<0.0001$), with the epicentre significantly greater than cranial and caudal regions ($p<0.0001$) for grey and white matter (denoted by #). Grey and white matter were not significantly different in any region ($p=0.08$). **(B)** For the 20cm SCI, a significant main effect for region was observed ($p<0.0001$), with the epicentre significantly elevated to cranial and caudal regions for both grey and white matter ($p<0.0001$) (denoted by #). There was a significant main effect between grey and white matter ($p=0.047$), which was in the caudal region ($p=0.01$).

IBA-1 Immunoreactivity

When examining IBA-1 immunoreactivity at varying spinal cord locations (Figure 14), there was a significant main effect between severity groups ($p<0.0001$). For the 20cm SCI, microglial expression greater than sham at 5cm ($p=0.02$) and 1cm ($p=0.03$) cranially, and at the epicentre ($p=0.003$). The 10cm SCI was significantly greater than sham at the epicentre ($p<0.0001$) and 1cm caudally ($p=0.03$). No significant differences were observed between 10cm and 20cm drop heights at any location.

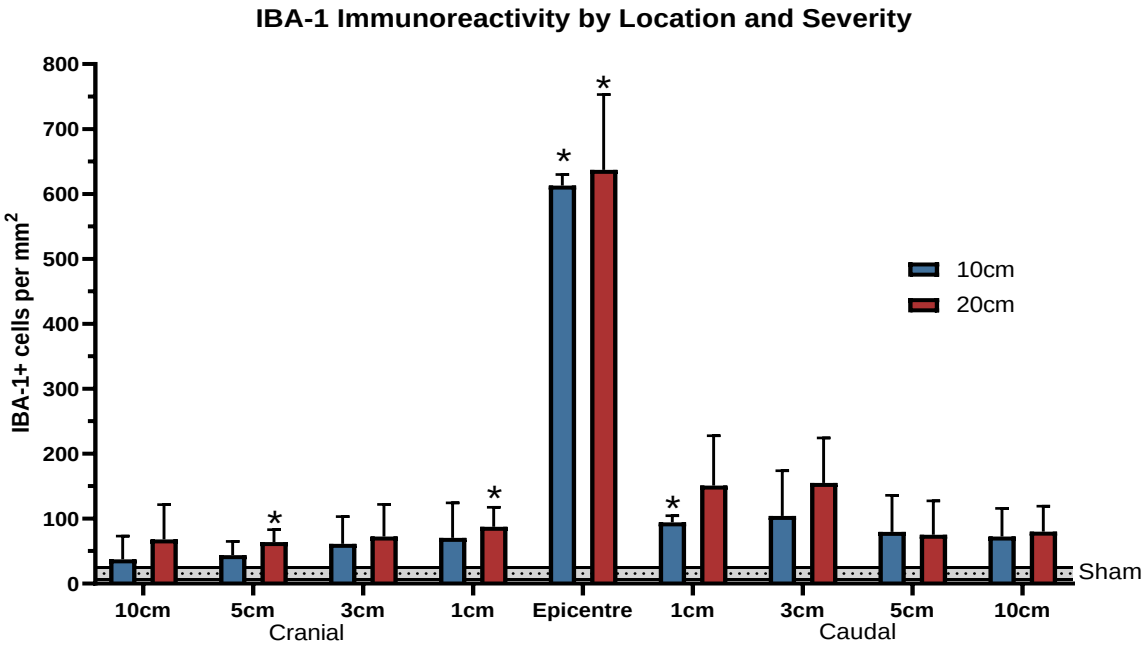

Figure 14: IBA-1 immunoreactivity at varying spinal cord locations. A repeated-measures two-way ANOVA revealed a significant main effect of SCI severity ($p<0.0001$), with the 20cm SCI significantly greater than sham at 5cm ($p=0.02$) and 1cm ($p=0.03$) cranially and at the epicentre ($p=0.003$). The 10cm SCI was significantly greater than sham at the epicentre ($p<0.0001$) and 1cm caudally ($p=0.001$). There were no significant differences between 20cm and 10cm drop heights at any region. * denotes significant difference to sham.

Grey and White Matter IBA-1 Immunoreactivity

We further examined IBA-1 immunoreactivity in grey and white matter regions to elucidate any differences between these tissues. The epicentre region was excluded from this analysis as the tissue disruption made it impossible to accurately identify specific regions. SCI severities were significantly elevated compared to sham in the grey matter (20cm: $p<0.0001$, 10cm: $p=0.004$) and white matter (20cm: $p=0.009$, 10cm: $p=0.049$) (Figure 15). There were no significant differences between severity groups; however, grey matter microglial expression for the 20cm SCI was significantly greater than white matter ($p=0.002$). There were no significant differences between grey matter anatomical regions ($p=0.08$) (Figure 16A). However, within white matter regions, the dorsal white matter column

was significantly greater than the lateral (p=0.048) and ventral columns (p=0.04) in the 10cm SCI (Figure 16B).

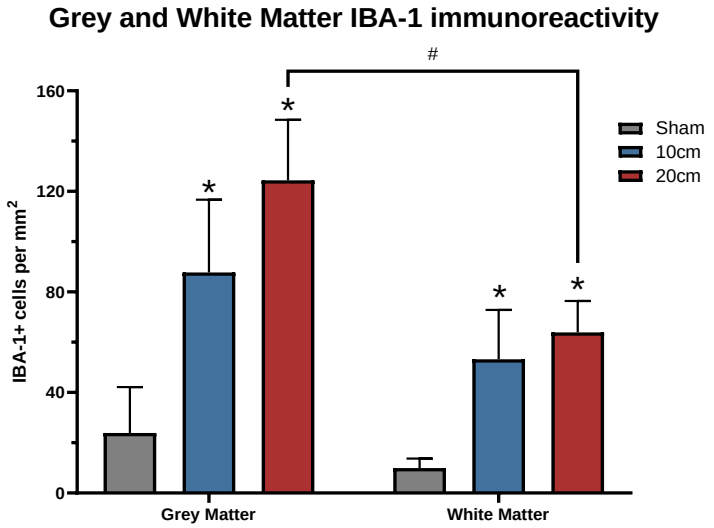

Figure 15: IBA-1 immunoreactivity in grey and white matter. A repeated measures two way ANOVA revealed a significant main effect of severity (p=0.002), with the 20cm (p<0.0001) and 10cm (p=0.004) groups significantly elevated compared to sham. There was a significant main effect for grey and white matter (p=0.0008), with grey matter significantly elevated for the 20cm SCI (p=0.002), but not for the 10cm (p=0.07) or sham (p=0.62) groups. * denotes significant differences to sham, # denotes significant difference between grey and white matter.

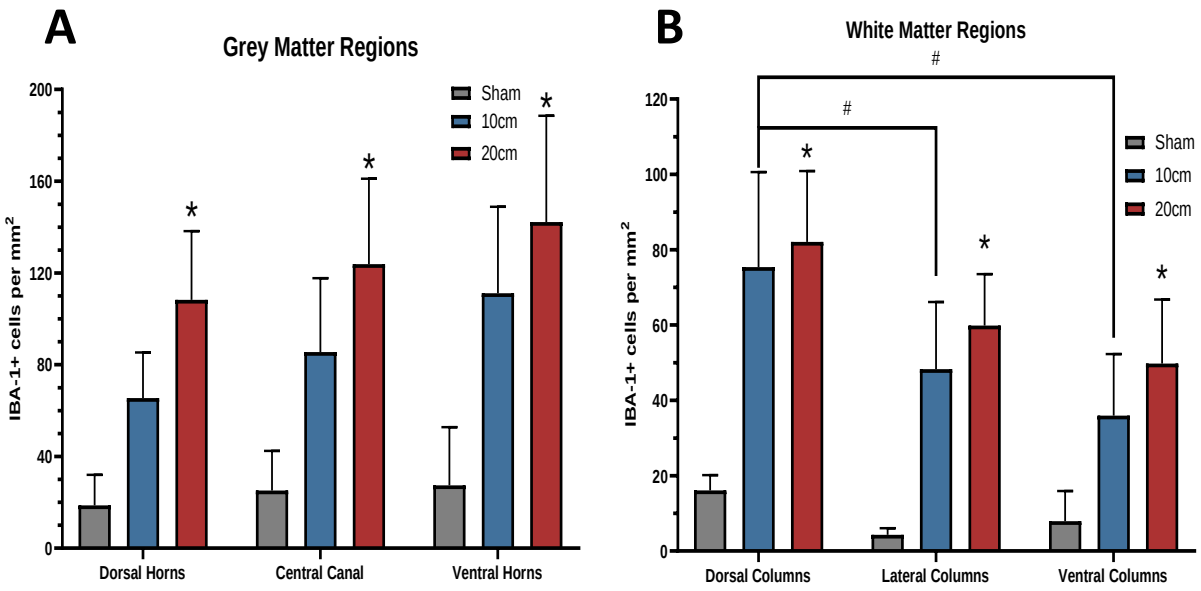

Figure 16: IBA-1 immunoreactivity in grey and white matter anatomical regions: **(A)** Within the grey matter, a repeated-measures two-way ANOVA revealed a significant main effect of severity ($p=0.03$), with the 20cm SCI significantly greater than sham at all regions (Dorsal horns: $p=0.011$, Central canal: $p=0.02$, Ventral horns: $p=0.03$). There were no significant differences between anatomical region ($p=0.08$). **(B)** In the white matter, there was a significant main effect of severity ($p=0.003$), which was between the 20cm and sham groups (Dorsal columns: $p=0.009$, lateral columns: $p=0.007$, ventral columns: $p=0.02$). There was a significant main effect of anatomical region ($p=0.001$), which was within the 10cm group between the dorsal column and the lateral ($p=0.048$) and ventral ($p=0.04$) columns.

Discussion

The present study examined tissue damage and microglial expression within our domestic porcine SCI model. We observed a significantly greater lesion volume after a 20cm SCI than a 10cm SCI, suggesting we successfully induced graded SCI severities that differed in total tissue damage. IBA-1 immunoreactivity for both severities was significantly greater than sham, but microglial expression did not differ between severities, refuting our hypothesis. Nonetheless, we successfully established the first porcine SCI model within Australia and characterised outcomes for varying SCI severities, demonstrating that our model is a viable research option.

We examined the extent of injury through tissue sparing and lesion volume analysis. Although lesion volume did not differ between severities in specific regions (cranial, epicentre, caudal), the 20cm SCI had a significantly greater total lesion volume than the 10cm. In line with this, a 10cm drop height had greater tissue sparing than a 20cm SCI in the University of British Columbia's (UBC) Yucatan miniature pig model[27]. Additionally, tissue damage appeared contained within 6.4mm cranially and caudally to the epicentre for the 10cm SCI in the UBC model, closely mirroring our findings[43]. This suggests that the relationship between impact force and tissue damage behaves similarly between both models, and indicates that our model may be a practical alternative.

Interestingly, comparisons of tissue damage within the UBC model have largely examined the cumulative percentage of tissue sparing, rather than lesion volume measurements[27, 43]. While this is a valid way to compare severities, there are several advantages to examining lesion volume[45]. Notably, the volumetric analysis facilitates comparisons to other stereological measurements[45, 46]. For example, our histological outcomes are directly comparable to in-vivo MRI measurements of lesion volume, which may directly translate to clinical practice[47]. Thus, our method of characterising injury severity is a strength of our study.

We then examined lesion volume to elucidate any differences between grey and white matter. Notably, grey matter lesion was significantly greater than white matter caudally for the 20cm SCI. As grey

matter has a considerably denser vasculature supply[48], we considered whether this finding was due to blood-spinal cord barrier (BSCB) permeability following injury. The BSCB is quickly compromised following SCI, causing an influx of proteins from the blood into the spinal cord and the formation of vasogenic oedema[49]. Interestingly, a rodent SCI study observed significant BSCB permeability up to 14 days post-SCI caudally to the injury site, but only up to 7 days post-SCI cranially[50]. Thus, the greater caudal grey matter lesion we observed may be due to the longer-lasting BSCB permeability in this region. We plan to investigate this possibility by examining BSCB integrity through albumin immunoreactivity.

An alternative explanation is that white matter damage may extend beyond 14-days post-SCI. Indeed, delayed Wallerian degeneration of neuronal axons in the white matter commencing as late as 24 days following a human SCI[51]. Thus, this significant difference may not be present at later time-points. Unfortunately, we only utilised a single time-point for tissue histology, meaning we are unable to confirm this possibility. Thus, a future direction is to examine lesion volume across multiple time points (24 hours, 3, 7, 14 and 21 days post-SCI) to discover temporal differences in grey and white matter lesion progression and elucidate potential mechanisms.

A limitation of our lesion volume analysis is that H&E-LFB staining reflects gross parenchymal damage rather than specific cell loss. Thus, further analysis may be warranted to provide a more detailed insight into the pattern of tissue damage[27]. For example, previous SCI research has examined the number of active neurons remaining through NeuN expression[52] , the extent of axonal injury through amyloid precursor protein[53], and the extent of apoptotic cell death through caspase-3 activity[54]. Combined, these markers would better characterise the impact of SCI severity on specific neuronal and cellular events. As such, we plan to utilise these markers in future analysis to comprehensively describe tissue damage within our model.

Next, we characterised the microglial response at 14-days post-SCI via IBA-1 immunoreactivity. As expected, IBA-1 immunoreactivity was significantly increased for both injury severities compared to

sham, particularly at the injury epicentre. This likely reflects an increased migration of microglia towards the injury epicentre, combined with a greater influx of circulating macrophages at this region[55]. Interestingly, IBA-1 immunoreactivity was not significantly different between severity groups as we had hypothesised. This was surprising, as microglia activation has previously been suggested to be severity-dependent[21]. However, as the spatial distribution of microglia appears to correlate with areas of necrotic or cystic damage[55, 56], it is possible that the locations we analysed were not ideal to distinguish between severity groups. Indeed, despite differing in total lesion volume, our percentage of tissue sparing analysis did not observe significant differences between drop heights at the injury epicentre. Thus, it may not be unexpected that both severity groups have a similar IBA-1 immunoreactivity within this region of similar tissue damage. We plan to further analyse microglial activity within the lesion site in a serialised manner similar to our lesion volume analysis, which may reveal a severity-depending IBA-1 immunoreactivity – particularly in the caudal region (2-7mm) where tissue sparing differs between groups.

Our further analysis of IBA-1 immunoreactivity revealed no significant differences between grey and white matter for sham or 10cm groups, but a significantly elevated IBA-1 immunoreactivity in the grey matter for the 20cm SCI. This may reflect the greater lesion volume observed in the grey matter caudally in the 20cm SCI group. When examining anatomical regions within the spinal cord, we observed a significantly elevated microglial response within the dorsal column of white matter for the 10cm SCI. This is potentially due to the dorsal direction of our SCI contusion that may cause more severe damage to this region and thus, a greater neuroinflammatory response. Indeed, a pronounced microglial expression in the dorsal columns was also observed following a dorsal contusion SCI in a rodent model[57], supporting this possible explanation.

Strengths and Limitations

The use of a porcine model of SCI was a major strength of this study. Due to the similarities in spinal anatomy and pathophysiology between pigs and humans, our results are highly translatable and

relevant to clinical practice. Despite this, our study was notably limited by the small sample size used. It has previously been recommended that porcine studies should utilise sample sizes of a minimum of 4-5 to have sufficient power[27], which was not achieved by our 10cm SCI group. Thus, we are limited in our ability to make any conclusive findings, particularly for this lower drop height group. While we acknowledge that this is a current limitation, this pilot study is ongoing and will address this in future analysis. Finally, our histological measures cannot be conducted in-vivo, which limits the translatability of our current findings. Despite this, we have also conducted in-vivo analysis through MRI imaging, functional assessments and blood serum analysis that will address this limitation in future studies.

Conclusion

This study demonstrated that graded SCI severities that differ in histological outcomes can be induced within our domestic pig model, and that the tissue outcomes within our model closely resembles pre-existing porcine literature at similar SCI drop heights. While we did not observe differences in microglial expression between severity groups, we have successfully established Australia's first porcine model of SCI, and have provided a robust foundation for future studies to utilise our model.

Word Count =4495

Professional & Funding Acknowledgments

Due to the nature of this study, a significant effort was made by a large number of people for this project to be conducted. We would like to acknowledge the following organisations and people for their contributions to the project:

SAHMRI PIRL facility, Adelaide Microscopy, National imaging facility, Translational Neuropathology Laboratory, Adelaide Spinal Research Group, Ms. Christine Gayen, Ms. Madeleine Bessen, Mr. Adnan Mulaibrahimovic, Dr. Anna Leonard, Dr. Claire Jones, Dr. Frances Corrigan, Dr. Ryan Doig, Dr. Ryan Quarrington, Prof. Brian Freeman.

Additionally, we would like to acknowledge the following funding bodies for their contributions to this project.

References

1. Tovell A (2019). Spinal cord injury, Australia, 2015-16. *Injury research and statistics series* **no. 122.** ,
2. Post M & Noreau L (2005). Quality of life after spinal cord injury. *J Neurol Phys Ther* **29**, 139-46.
3. Kwon BK, Tetzlaff W, Grauer JN, Beiner J & Vaccaro AR (2004). Pathophysiology and pharmacologic treatment of acute spinal cord injury. *Spine J* **4**, 451-64.
4. Tator CH (2006). Review of treatment trials in human spinal cord injury: issues, difficulties, and recommendations. *Neurosurgery* **59**, 957-82; discussion 982-7.
5. Oyinbo CA (2011). Secondary injury mechanisms in traumatic spinal cord injury: a nugget of this multiply cascade. *Acta Neurobiol Exp (Wars)* **71**, 281-99.
6. Kjell J & Olson L (2016). Rat models of spinal cord injury: from pathology to potential therapies. *Dis Model Mech* **9**, 1125-1137.
7. Kim KT, Streijger F, Manouchehri N, So K, Shortt K, Okon EB, Tigchelaar S, Cripton P & Kwon BK (2018). Review of the UBC Porcine Model of Traumatic Spinal Cord Injury. *J Korean Neurosurg Soc* **61**, 539-547.
8. Rowland JW, Hawryluk GW, Kwon B & Fehlings MG (2008). Current status of acute spinal cord injury pathophysiology and emerging therapies: promise on the horizon. *Neurosurg Focus* **25**, E2.
9. Alizadeh A, Dyck SM & Karimi-Abdolrezaee S (2019). Traumatic Spinal Cord Injury: An Overview of Pathophysiology, Models and Acute Injury Mechanisms. *Front Neurol* **10**, 282.
10. Little JW (2006). Spinal Cord Injury: Promise, Progress, and Priorities. *The Journal of Spinal Cord Medicine* **29**, 172-172.
11. Kreutzberg GW (1996). Microglia: a sensor for pathological events in the CNS. *Trends Neurosci* **19**, 312-8.
12. Davalos D, Grutzendler J, Yang G, Kim JV, Zuo Y, Jung S, Littman DR, Dustin ML & Gan WB (2005). ATP mediates rapid microglial response to local brain injury in vivo. *Nat Neurosci* **8**, 752-8.
13. Kroner A & Rosas Almanza J (2019). Role of microglia in spinal cord injury. *Neuroscience Letters* **709**, 134370.
14. Ren H, Chen X, Tian M, Zhou J, Ouyang H & Zhang Z (2018). Regulation of Inflammatory Cytokines for Spinal Cord Injury Repair Through Local Delivery of Therapeutic Agents. *Advanced Science* **5**, 1800529.
15. Clarity T (2019). Acute social defeat-induced neuroinflammation in the vmPFC of Syrian hamsters via microglial activation.
16. Orr MB & Gensel JC (2018). Spinal Cord Injury Scarring and Inflammation: Therapies Targeting Glial and Inflammatory Responses. *Neurotherapeutics* **15**, 541-553.
17. Murphy MP (1999). Nitric oxide and cell death. *Biochimica et Biophysica Acta (BBA) - Bioenergetics* **1411**, 401-414.
18. Kawabori M & Yenari MA (2015). The role of the microglia in acute CNS injury. *Metabolic brain disease* **30**, 381-392.
19. David S & Kroner A (2011). Repertoire of microglial and macrophage responses after spinal cord injury. *Nature Reviews Neuroscience* **12**, 388-399.
20. Alexander JK & Popovich PG (2009). Neuroinflammation in spinal cord injury: therapeutic targets for neuroprotection and regeneration. In *Progress in Brain Research*, edn, ed. Verhaagen J, Hol EM, Huitenga I, Wijnholds J, Bergen AB, Boer GJ & Swaab DF, 125-137. Elsevier.
21. Akhmetzyanova E, Kletenkov K, Mukhamedshina Y & Rizvanov A (2019). Different Approaches to Modulation of Microglia Phenotypes After Spinal Cord Injury. *Frontiers in Systems Neuroscience* **13**,
22. Kwon BK, Streijger F, Hill CE, Anderson AJ, Bacon M, Beattie MS, Blesch A, Bradbury EJ, Brown A, Bresnahan JC, Case CC, Colburn RW, David S, Fawcett JW, Ferguson AR, Fischer I, Floyd CL, Gensel JC, Houle JD, Jakeman LB, Jeffery ND, Jones LA, Kleitman N, Kocsis J, Lu P, Magnuson DS, Marsala M, Moore SW, Mothe AJ, Oudega M, Plant GW, Rabchevsky AS, Schwab JM, Silver J, Steward O, Xu XM, Guest JD & Tetzlaff W (2015). Large animal and primate models of spinal cord injury for the testing of novel therapies. *Exp Neurol* **269**, 154-68.
23. Biglari B, Swing T, Child C, Büchler A, Westhauser F, Bruckner T, Ferbert T, Jürgen Gerner H & Moghaddam A (2015). A pilot study on temporal changes in IL-1β and TNF-α serum levels after spinal

cord injury: the serum level of TNF-α in acute SCI patients as a possible marker for neurological remission. *Spinal Cord* **53**, 510-4.
24. Stammers AT, Liu J & Kwon BK (2012). Expression of inflammatory cytokines following acute spinal cord injury in a rodent model. *J Neurosci Res* **90**, 782-90.
25. Agoston DV, Vink R, Helmy A, Risling M, Nelson D & Prins M (2019). How to Translate Time: The Temporal Aspects of Rodent and Human Pathobiological Processes in Traumatic Brain Injury. *J Neurotrauma* **36**, 1724-1737.
26. Kim K-T, Streijger F, Manouchehri N, So K, Shortt K, Okon EB, Tigchelaar S, Cripton P & Kwon BK (2018). Review of the UBC Porcine Model of Traumatic Spinal Cord Injury. *Journal of Korean Neurosurgical Society* **61**, 539-547.
27. Lee JH, Jones CF, Okon EB, Anderson L, Tigchelaar S, Kooner P, Godbey T, Chua B, Gray G, Hildebrandt R, Cripton P, Tetzlaff W & Kwon BK (2013). A novel porcine model of traumatic thoracic spinal cord injury. *J Neurotrauma* **30**, 142-59.
28. Mair KH, Sedlak C, Kaser T, Pasternak A, Levast B, Gerner W, Saalmuller A, Summerfield A, Gerdts V, Wilson HL & Meurens F (2014). The porcine innate immune system: an update. *Dev Comp Immunol* **45**, 321-43.
29. Schomberg DT, Miranpuri GS, Chopra A, Patel K, Meudt JJ, Tellez A, Resnick DK & Shanmuganayagam D (2017). Translational Relevance of Swine Models of Spinal Cord Injury. *J Neurotrauma* **34**, 541-551.
30. Hu S, Chao CC, Khanna KV, Gekker G, Peterson PK & Molitor TW (1996). Cytokine and free radical production by porcine microglia. *Clin Immunol Immunopathol* **78**, 93-6.
31. Rubic-Schneider T, Christen B, Brees D & Kammuller M (2016). Minipigs in Translational Immunosafety Sciences: A Perspective. *Toxicol Pathol* **44**, 315-24.
32. Neirinckx V, Coste C, Franzen R, Gothot A, Rogister B & Wislet S (2014). Neutrophil contribution to spinal cord injury and repair. *J Neuroinflammation* **11**, 150.
33. Sheng SR, Wang XY, Xu HZ, Zhu GQ & Zhou YF (2010). Anatomy of large animal spines and its comparison to the human spine: a systematic review. *Eur Spine J* **19**, 46-56.
34. Leonard AV, Menendez JY, Pat BM, Hadley MN & Floyd CL (2017). Localization of the corticospinal tract within the porcine spinal cord: Implications for experimental modeling of traumatic spinal cord injury. *Neurosci Lett* **648**, 1-7.
35. (2017). Translational Relevance of Swine Models of Spinal Cord Injury. *Journal of Neurotrauma* **34**, 541-551.
36. Sharif-Alhoseini M, Khormali M, Rezaei M, Safdarian M, Hajighadery A, Khalatbari MM, Safdarian M, Meknatkhah S, Rezvan M, Chalangari M, Derakhshan P & Rahimi-Movaghar V (2017). Animal models of spinal cord injury: a systematic review. *Spinal Cord* **55**, 714-721.
37. Gutierrez K, Dicks N, Glanzner WG, Agellon LB & Bordignon V (2015). Efficacy of the porcine species in biomedical research. *Front Genet* **6**, 293.
38. Foditsch EE, Miclaus G, Patras I, Hutu I, Roider K, Bauer S, Janetschek G, Aigner L & Zimmermann R (2018). A new technique for minimal invasive complete spinal cord injury in minipigs. *Acta Neurochir (Wien)* **160**, 459-465.
39. Nardone R, Florea C, Höller Y, Brigo F, Versace V, Lochner P, Golaszewski S & Trinka E (2017). Rodent, large animal and non-human primate models of spinal cord injury. *Zoology (Jena)* **123**, 101-114.
40. Zhang N, Yin Y, Xu S-J, Wu Y-P & Chen W-S (2012). Inflammation & apoptosis in spinal cord injury. *The Indian journal of medical research* **135**, 287-296.
41. Lombardo C, Damiano G, Cassata G, Palumbo VD, Cacciabaudo F, Spinelii G, Calvagna C, Gioviale MC, Maione CL & Lo Monte AI (2010). Surgical vascular access in the porcine model for long-term repeated blood sampling. *Acta Biomed* **81**, 101-3.
42. Bozkus H, Crawford NR, Chamberlain RH, Valenzuela TD, Espinoza A, Yüksel Z & Dickman CA (2005). Comparative anatomy of the porcine and human thoracic spines with reference to thoracoscopic surgical techniques. *Surgical Endoscopy And Other Interventional Techniques* **19**, 1652-1665.
43. Tigchelaar S, Streijger F, Sinha S, Flibotte S, Manouchehri N, So K, Shortt K, Okon E, Rizzuto MA, Malenica I, Courtright-Lim A, Eisen A, Keuren-Jensen KV, Nislow C & Kwon BK (2017). Serum MicroRNAs Reflect Injury Severity in a Large Animal Model of Thoracic Spinal Cord Injury. *Sci Rep* **7**, 1376.

44. Bankhead P, Loughrey MB, Fernández JA, Dombrowski Y, McArt DG, Dunne PD, McQuaid S, Gray RT, Murray LJ, Coleman HG, James JA, Salto-Tellez M & Hamilton PW (2017). QuPath: Open source software for digital pathology image analysis. *Scientific Reports* **7**, 16878.
45. Jakeman LB (2012). Assessment of Lesion and Tissue Sparing Volumes Following Spinal Cord Injury. In *Animal Models of Acute Neurological Injuries II: Injury and Mechanistic Assessments, Volume 2*, edn, ed. Chen J, Xu X-M, Xu ZC & Zhang JH, 417-442. Humana Press, Totowa, NJ.
46. White RE, McTigue DM & Jakeman LB (2010). Regional heterogeneity in astrocyte responses following contusive spinal cord injury in mice. *The Journal of comparative neurology* **518**, 1370-1390.
47. David SD, Sunil J, Jason C, Colin K, Paula JF & Lynne CW (2008). Magnetic resonance imaging versus histological assessment for estimation of lesion volume after experimental spinal cord injury. *Journal of Neurosurgery: Spine SPI* **9**, 301-306.
48. Halder SK, Kant R & Milner R (2018). Chronic mild hypoxia promotes profound vascular remodeling in spinal cord blood vessels, preferentially in white matter, via an α5β1 integrin-mediated mechanism. *Angiogenesis* **21**, 251-266.
49. Bartanusz V, Jezova D, Alajajian B & Digicaylioglu M (2011). The blood-spinal cord barrier: morphology and clinical implications. *Ann Neurol* **70**, 194-206.
50. Whetstone WD, Hsu JY, Eisenberg M, Werb Z & Noble-Haeusslein LJ (2003). Blood-spinal cord barrier after spinal cord injury: relation to revascularization and wound healing. *J Neurosci Res* **74**, 227-39.
51. Buss A, Brook GA, Kakulas B, Martin D, Franzen R, Schoenen J, Noth J & Schmitt AB (2004). Gradual loss of myelin and formation of an astrocytic scar during Wallerian degeneration in the human spinal cord. *Brain* **127**, 34-44.
52. Ek CJ, Habgood MD, Callaway JK, Dennis R, Dziegielewska KM, Johansson PA, Potter A, Wheaton B & Saunders NR (2010). Spatio-Temporal Progression of Grey and White Matter Damage Following Contusion Injury in Rat Spinal Cord. *PLOS ONE* **5**, e12021.
53. Medana IM & Esiri MM (2003). Axonal damage: a key predictor of outcome in human CNS diseases. *Brain* **126**, 515-530.
54. Springer JE, Azbill RD & Knapp PE (1999). Activation of the caspase-3 apoptotic cascade in traumatic spinal cord injury. *Nature Medicine* **5**, 943-946.
55. Zhou X, He X & Ren Y (2014). Function of microglia and macrophages in secondary damage after spinal cord injury. *Neural Regeneration Research* **9**, 1787-1795.
56. Fleming JC, Norenberg MD, Ramsay DA, Dekaban GA, Marcillo AE, Saenz AD, Pasquale-Styles M, Dietrich WD & Weaver LC (2006). The cellular inflammatory response in human spinal cords after injury. *Brain* **129**, 3249-3269.
57. Popovich PG, Wei P & Stokes BT (1997). Cellular inflammatory response after spinal cord injury in Sprague-Dawley and Lewis rats. *J Comp Neurol* **377**, 443-64.